© 2016. Published by The Company of Biologists Ltd | Journal of Cell Science (2016) 129, 430-443 doi:10.1242/jcs.179200

RESEARCH ARTICLE

Rop, the Sec1/Munc18 homolog in *Drosophila*, is required for furrow ingression and stable cell shape during cytokinesis

Heather DeBruhl[1,*], Roger Albertson[2], Zachary Swider[1] and William Sullivan[1,‡]

ABSTRACT

Physically separating daughter cells during cytokinesis requires contraction of an actin-myosin ring and vesicle-mediated membrane addition at the cleavage furrow. To identify vesicle trafficking proteins that function in cytokinesis, we screened deficiencies and mutations of candidate genes by live imaging the mitotic domains of the *Drosophila* embryo. In embryos homozygous for some of these deficiencies, we observed several cytokinesis phenotypes, including slow furrow ingression and increased membrane blebbing. We also found that cytokinesis required the Sec1/Munc18 homolog Rop, which interacts with syntaxin and mediates exocytosis at the plasma membrane. In a temperature-sensitive *Rop* mutant (Rop^{TS}), the contractile ring disassembled during furrow ingression, indicating that maintenance of the ring required vesicle addition. Furthermore, in some dividing Rop^{TS} cells, the shape of the daughter cells became unstable, causing cytokinesis failure. These results further highlight the importance of vesicle trafficking in animal cytokinesis and show that vesicle fusion influences cell shape during cytokinesis.

KEY WORDS: Sec1/Munc18, Rop, Cytokinesis, Vesicle trafficking

INTRODUCTION

Vesicle trafficking plays an essential role in animal cytokinesis, the physical separation of daughter cells after mitosis. To maintain a constant cell volume through multiple rounds of cell division, new membrane must be added. In *Xenopus*, zebrafish and *Drosophila* embryos, researchers have observed vesicles delivered to the cleavage furrow during cytokinesis, suggesting that such membrane addition occurs at the site of division (Danilchik et al., 2003; Li et al., 2006; Albertson et al., 2008). Furthermore, mutation or inhibition of Golgi, endosomal and other vesicle trafficking components disrupts furrow ingression or abscission, showing that vesicle transport is essential at multiple steps of cytokinesis (Albertson et al., 2005; McKay and Burgess, 2011). In addition to general membrane, vesicle transport might also deliver Rho guanine nucleotide exchange factors (GEFs) and other factors that influence cortical cytoskeletal dynamics to the site of furrow ingression (Cao et al., 2008; Dambournet et al., 2011; Schiel et al., 2012).

Although many conserved components of cytokinesis have been identified, recent screens continue to identify new roles for proteins in cytokinesis, suggesting that more components remain undiscovered (Eggert et al., 2006; Slack et al., 2006; Gregory et al., 2007; Hyodo et al., 2012; Zhang et al., 2012). Three cell-culture-based screens – a proteomics analysis of the mammalian midbody and two RNA interference (RNAi) screens using *Drosophila* S2 cells – as well as a genetic screen in *Drosophila* spermatocytes have highlighted the importance of vesicle trafficking genes in cytokinesis (Echard et al., 2004; Eggert et al., 2004; Skop et al., 2004; Giansanti and Fuller, 2012). However, these cell-culture-based screens failed to identify vesicle trafficking components, such as Rab11, already known to function in cytokinesis *in vivo* (Skop et al., 2001; Wilson et al., 2005; Giansanti et al., 2007). Taken together, these results suggest that vesicle trafficking components important for cytokinesis remain undiscovered and emphasize the importance of screens *in vivo*.

In addition to screens, many functional studies of vesicle trafficking proteins in cytokinesis have also been performed in cell culture (McKay and Burgess, 2011). In contrast, in epithelial tissue, neighboring cells exert forces and stresses on each other (Mao and Baum, 2015). What role vesicle trafficking proteins play in cytokinesis in such a complex environment remains unknown. Compared to cytokinesis in cell culture, cytokinesis might require additional unidentified factors within an epithelium.

To examine the role of vesicle addition during cytokinesis in epithelial tissue, here, we conducted a live-imaging-based screen of mitotic divisions in the *Drosophila* embryo. These divisions occur directly after cellularization (Fig. 1A). During mitosis of cycle 14, cells with similar differentiation commitments divide synchronously in stereotypical clusters of cells called mitotic domains (Fig. 1B,C) (Foe, 1989). Because these clusters of cells divide rapidly and reside at the embryo surface, furrow formation, ingression and abscission are easily imaged live. Such live imaging reveals at what stage cytokinesis fails at and detects phenotypes more subtle than failure, which are missed by a single time-point fixed analysis. Importantly, vesicle delivery to the ingressing furrow occurs in these cells, suggesting an important role for vesicle trafficking in cytokinesis in this cell type (Albertson et al., 2008).

To identify and characterize vesicle trafficking genes and other factors important for cytokinesis, we screened embryos homozygous for either deficiencies or mutations in candidate genes for defects in cytokinesis during cycle 14. The first 13 mitotic divisions in the *Drosophila* embryo occur within a syncytium, followed by cellularization, which individualizes nuclei into cells (Fig. 1A) (Foe et al., 1993). These early events are driven by maternally loaded mRNAs and proteins. Previous genome-wide deficiency screens have revealed that nuclear cycles 1–13 do not require expression of zygotic genes. These screens have also demonstrated that successful cellularization only requires expression of seven zygotic genes (Merrill et al., 1988; Wieschaus and Sweeton, 1988). Here, we use this same approach to screen for genes whose zygotic expression is required for the events immediately following cellularization, specifically the first

[1]Molecular, Cell and Developmental Biology, University of California at Santa Cruz, Santa Cruz, CA 95064, USA. [2]Biology Department, Albion College, Albion, MI 49224, USA.
*Present address: Biological Sciences, California Polytechnic State University, San Luis Obsipo, CA 93407, USA.

‡Author for correspondence (sullivan@biology.ucsc.edu)

Received 24 August 2015; Accepted 30 November 2015

Journal of Cell Science (2016) 129, 430-443 doi:10.1242/jcs.179200

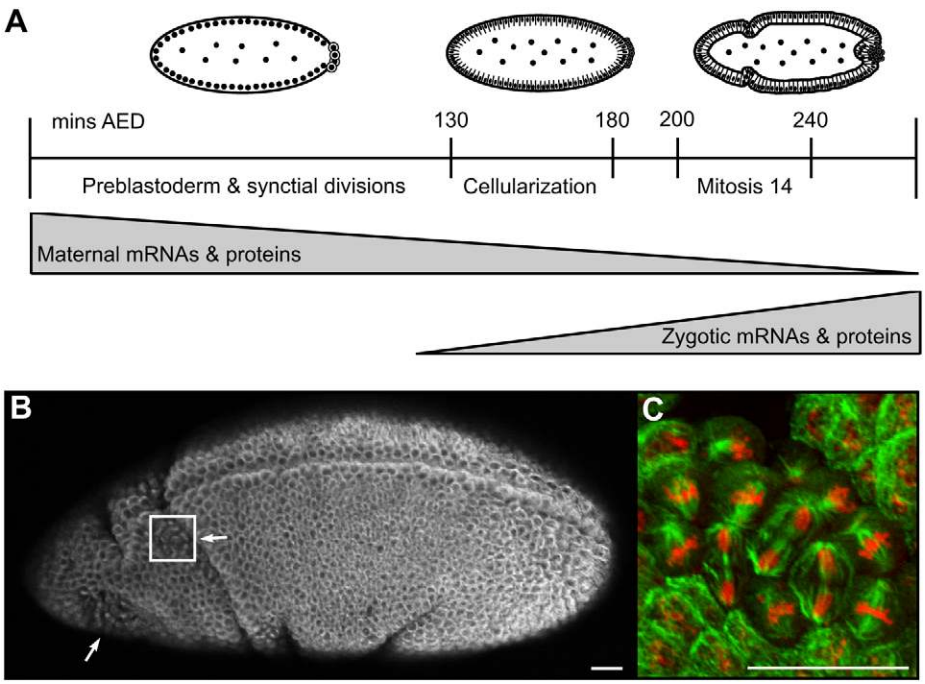

Fig. 1. Mitotic domains in early *Drosophila* embryos. (A) Schematic of early stages of embryogenesis. The time line indicates the development timing in minutes after egg deposition (AED) at 25°C (Foe et al., 1993). Above the graph, line drawings (styled after Foe and Alberts, 1983) show embryo morphology at different stages. Shaped triangles below the time line represent relative levels of maternally loaded versus zygotically produced mRNAs and proteins. (B) Immunofluorescence image of anti-tubulin antibody staining in a fixed cycle 14 embryo. Anterior on the left, ventral at the top. Box indicates the area shown in panel C. Arrows indicate two mitotic domains. (C) Immunofluorescence image of cycle 14 mitotic domain. Anti-tubulin antibody staining (green) marks mitotic spindles and midbodies. DNA staining (red) marks chromosomes. Note cells in metaphase, anaphase and telophase. Scale bars: 25 µm.

conventional cytokinesis that occurs during anaphase and telophase of nuclear cycle 14 (Fig. 1A).

We identified three deficiencies on the third chromosome that exhibited unique cytokinesis phenotypes, including increased blebbing during cytokinesis. By testing known vesicle trafficking mutants for cytokinesis defects, we additionally found that cytokinesis required the syntaxin-interacting protein Rop (also known as Sec1 or Munc18 in other systems). Disruption of Rop function caused furrow regression and destabilized cell shape during cytokinesis, highlighting the importance of exocytosis in cytokinesis.

RESULTS

A genetic screen *in vivo* for vesicle trafficking components important for cytokinesis

We set out to identify vesicle trafficking genes important for cytokinesis *in vivo* using the mitotic domains of the *Drosophila* embryo. These divisions occur immediately after cellularization, during the transition from maternal to zygotic control of cell division (Fig. 1A). In these mitotic domains, cells divide sequentially, allowing continuous filming of multiple divisions (Fig. 1B,C). For our analysis, we primarily focused on mitotic domains in the anterior head region. To visualize cytokinesis live, we used the GAL4–UAS system to maternally load embryos with Synaptotagmin–GFP (Syt–GFP), a neuronal membrane protein that, when ectopically expressed, marks the plasma membrane (Fig. 2A,B, left panel) (Zhang et al., 2002; Albertson et al., 2008). To identify embryos homozygous for each deficiency studied, we crossed heterozygous parents and selected against the cytoplasmic GFP expressed by a *twist-GAL4, UAS-GFP* cassette on the balancer chromosome (Fig. 2A,B). We then assessed homozygous deficiency lines by live imaging for failed cell divisions and abnormal furrow ingression.

Control experiments demonstrated the advantages of this system. First, we previously used this same crossing scheme with *pbl/Ect2*, the cytokinesis Rho-GEF, and identified homozygous *pbl* mutants with disrupted furrow ingression (Albertson et al., 2008). Second, we examined *nullo* – a zygotic gene required for partitioning a single nucleus into each cell during cellularization (Wieschaus and Sweeton, 1988; Simpson and Wieschaus, 1990). Consistently, we found that either a homozygous *nullo* mutation or a homozygous deficiency that includes *nullo* caused multinucleate cells after cellularization, prior to cycle 14 of mitosis (Fig. 2C, Table S1; R.A., unpublished data). Thus, this system detected a known cytokinesis factor and recapitulated previously published results. However, our screen will not recover cytokinesis proteins with sufficient maternally loaded protein and mRNA stores. For example, embryos homozygous for the deficiency *Df(1)v-L15*, which includes the essential cytokinesis gene *fascetto/PRC1*, appeared normal, suggesting that maternally loaded PRC1 is sufficient for cycle 14 divisions (Fig. 2C, Table S1). As in many screens, conclusions cannot be drawn from negative results.

Cytokinesis defects identified in deficiency lines

In our screen, we identified cytokinesis defects in three out of the 15 experimental deficiency lines assayed, which covered ∼4% and ∼15% of the X and third chromosomes, respectively (Fig. 2C; Table S1). In wild-type embryos, cytokinesis always proceeded normally (n=50 cells from four embryos). Cytokinesis furrows initiated (time 0 s), ingressed (arrowheads), closed and remained closed as expected (Fig. 2D; Movie 1). We observed both symmetric and asymmetric furrow ingression, where in the latter the furrow ingressed from only one side. Such asymmetric furrows have been previously noted in embryonic divisions of many species (Rappaport, 1996).

Df(3L)R-G5 embryos displayed striking ectopic membrane blebbing during cytokinesis (Fig. 2E; Movie 2). Membrane blebs – protrusions in the membrane – commonly form at the cell poles during cytokinesis (Charras, 2008). In wild-type embryos, we observed such polar membrane blebs during cytokinesis in 17% of cells (n=23 cells from two embryos). *Df(3L)R-G5* embryos carry a 617-kb deletion encoding about 90 genes. In these embryos, 53% of cells in cytokinesis (n=38 cells from two embryos) had at least one

Journal of Cell Science (2016) 129, 430-443 doi:10.1242/jcs.179200

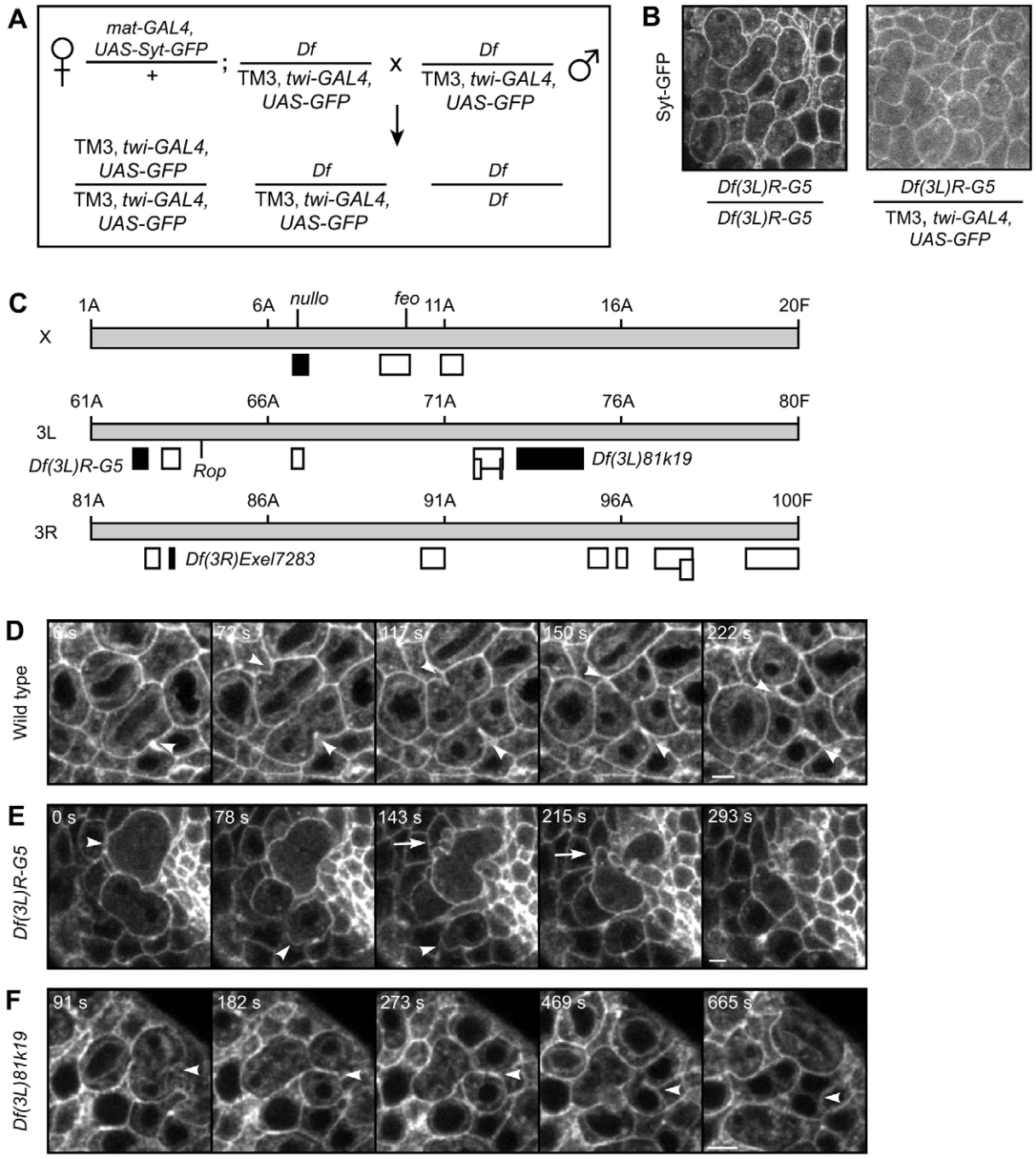

Fig. 2. Cytokinesis defects identified in a live-imaging screen of *Drosophila* embryos. (A) Genotypes and crossing scheme used to create homozygous deficiency embryos maternally loaded with Synaptotagmin–GFP (Syt–GFP). *mat-GAL4* drives maternal loading, *twist(twi)-GAL4* drives embryonic expression. (B) GFP signal of mitotic domains in cycle 14 embryos either homozygous or heterozygous for *Df(3L)R-G5*. Homozygous embryos were identified by the absence of ubiquitous cytoplasmic GFP from the *twist-GAL4, UAS-GFP* balancer chromosome. Maternally loaded Syt–GFP marks cell membranes in both embryos. (C) Diagram of the X and third chromosomes, shown as gray boxes, with cytological numbers indicated above. Boxes below the chromosomes depict the deficiency lines screened. Black indicates phenotype observed. White indicates no phenotype. Location of the three genes *nullo*, *feo* and *Rop* are also noted. (D–F) Time-lapse images of Syt–GFP in cycle 14 mitotic domains of wild-type (D, Movie 1), *Df(3R)R-G5* (E, Movie 2) and *Df(3L)81k19* (F) embryos. Syt–GFP marks the plasma membrane and ingressing furrow. The time from the beginning of furrow initiation to the first cell dividing is indicated. (D) Normal furrow ingression (arrowheads) in wild-type cells. (E) In *Df(3L)R-G5* embryos, cells undergoing cytokinesis displayed abnormally large membrane blebs (arrowheads) and ectopic blebs at the furrow (arrow). (F) In *Df(3L)81k19* embryos, cytokinesis furrows regressed (arrowheads). Scale bars: 5 µm.

membrane bleb. Interestingly, in *Df(3L)R-G5* embryos the cytokinesis blebs formed both at the cell poles and the cleavage furrow. In an extreme example, one dividing cell (Fig. 2E; Movie 2) formed many large membrane blebs at the ingressing furrow, similar to S2 cells depleted of the cytokinesis protein anillin (Somma et al., 2002; Echard et al., 2004).

Another large deficiency, *Df(3L)81k19*, which deletes about 1.25 Mb, caused binucleate cells in multiple embryos. Live-

Journal of Cell Science (2016) 129, 430-443 doi:10.1242/jcs.179200

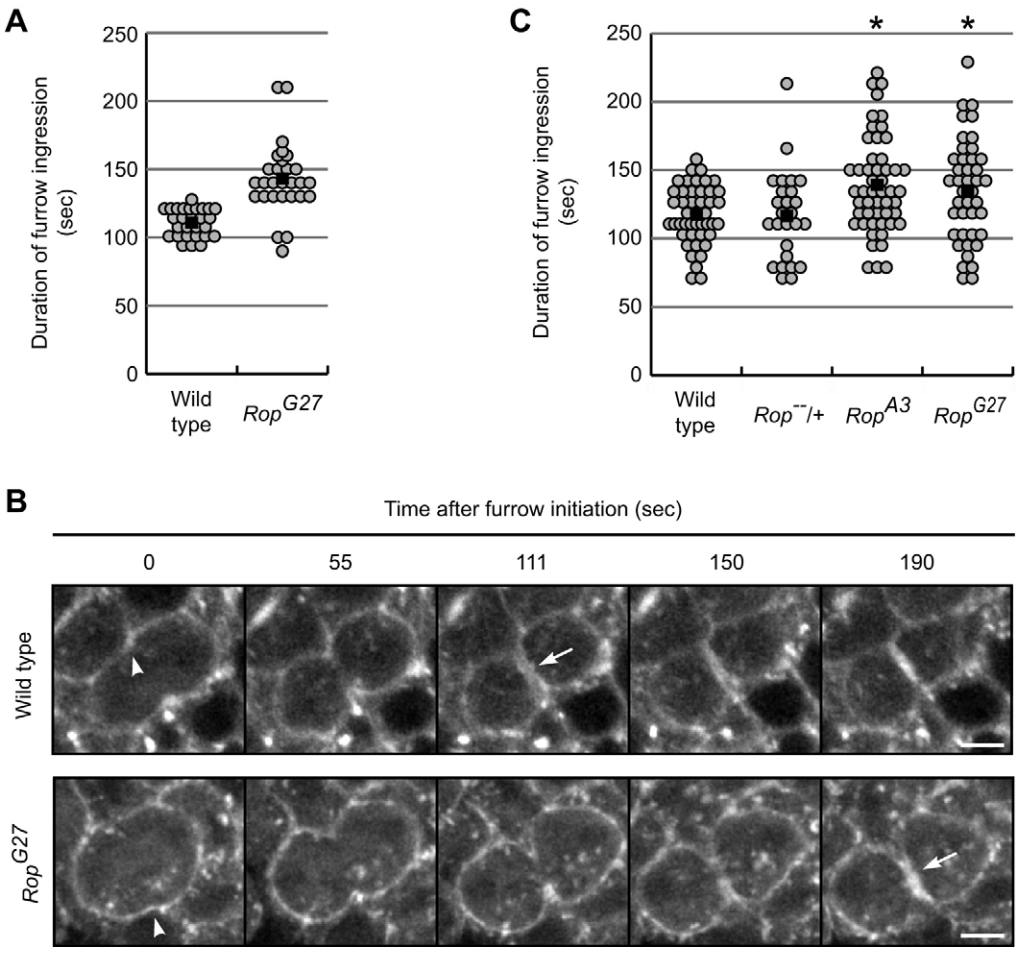

Fig. 3. Slow furrow ingression in *Rop*-mutant embryos. (A,C) Graphs of timing of furrow ingression during cytokinesis in wild-type, *Rop* heterozygous and *Rop* mutant embryos. The duration of furrow ingression was measured from initiation to completion using Synaptotagmin–GFP (A) or Rhodamine–actin (C) to mark the cell membrane and ingressing furrow. Each circle represents timing for a single cell. Black bars mark the average mean time for each genotype. **P*<0.01 from wild-type (*t*-test). Data were from *n* embryos for each genotype: (A) wild type, 3; Rop^{G27}, 2; (C) wild type, 3; *Rop* heterozygous, 3; Rop^{A3}, 4; Rop^{G27}, 3. (B) Time-lapse images of fluorescently labeled actin from live imaging of cytokinesis in wild-type (yw^{67}) and *Rop* mutant embryos. Arrowheads mark the first indentation of the cleavage furrow, defined as furrow initiation. Arrows mark furrow completion when opposing sides of the ingressing furrow meet. Scale bars: 5 µm.

imaging revealed furrow regression in 9.8% of cells (n=82 cells from seven embryos) (Fig. 2F), significantly different from the perfect success rate observed in wild-type embryos (n=50 cells from four embryos) (Fisher's exact test, P=0.024).

Finally, we observed a slow ingression phenotype in *Df(3R)Exel7283* embryos. Using the Syt–GFP, we measured the duration of furrow ingression from initiation – the first indentation at the cleavage furrow – to completion – closure of the furrow gap. In *Df(3R)Exel7283* embryos, cells took longer to complete furrow ingression [145.7±22.1 s (n=13 cells from two embryos) versus 110.9±10.1 s in wild-type (n=28 cells from four embryos); mean± s.e.m.]. Thus, although cytokinesis never failed, furrow ingression was slower. This 98-kb deficiency deletes 17 genes, including the vesicle trafficking gene *Sec23*. However, analysis of *Sec23*-null embryos did not recapitulate the slow furrow ingression phenotype (H.D., Z.S., unpublished data), suggesting that another gene within the deficiency is responsible.

Slow furrow ingression during cytokinesis in Rop-null embryos

In addition to deficiency lines, we also tested vesicle trafficking mutants for cytokinesis defects using this system. We focused on vesicle trafficking genes previously identified in cytokinesis cell culture screens to confirm those results *in vivo* and characterize their role in cytokinesis in an epithelial tissue where cells experience external forces. First, we tested the COPII coat protein Sec13, which is required for cytokinesis in the early *C. elegans* embryo (Skop et al., 2004). However, homozygous *Sec13* mutant *Drosophila* embryos displayed normal cytokinesis during cycle 14 (R.A., unpublished observation), suggesting that maternally loaded Sec13 was sufficient in our system.

Next, we tested and identified a cytokinesis defect in *Rop* mutant embryos and, as described in the remainder of this report, characterized the role of Rop in cytokinesis. *Rop* is the *Drosophila* homolog of yeast *SEC1* (Salzberg et al., 1993). Sec1/Munc18-like (SM) proteins are essential components of SNARE-mediated membrane fusion – they regulate activity of the trans-SNARE complex (Sudhof and Rothman, 2009). In *Drosophila*, Rop functions in both general secretion and neurotransmitter release by interacting with the t-SNARE syntaxin and regulating vesicle fusion with the plasma membrane (Harrison et al., 1994; Halachmi et al., 1995; Wu et al., 1998). SM proteins are cytoplasmic (Sudhof and Rothman, 2009). Consistent with this, in the cycle 14 mitotic domains, Rop exhibited a punctate distribution in the cytoplasm that sometimes colocalized with the cell cortex (Fig. S1) (n=21 cells from four embryos).

Live imaging using the Syt–GFP showed that furrow ingression from initiation to completion took on average 1.3 times longer in zygotic *Rop*-null cells than wild-type cells (Fig. 3A), suggesting that Rop can also play a role in vesicle-mediated membrane addition during cytokinesis. We confirmed these results by injecting fluorescently labeled actin into wild-type and *Rop* mutant embryos, to mark the cell cortex and ingressing furrow. Timing analysis from furrow initiation (Fig. 3B, arrowhead) to completion (Fig. 3B, arrow) again showed that *Rop*-null cells had significantly longer furrow ingression than wild-type or heterozygous controls

Journal of Cell Science (2016) 129, 430-443 doi:10.1242/jcs.179200

(*t*-test, $P<0.01$) (Fig. 3C). Importantly, two different *Rop*-null alleles gave similar results, demonstrating that the defect was caused by mutation of *Rop* and not a background mutation. Finally, although furrows ingressed slowly, their morphology appeared otherwise normal (Fig. 3B).

Characterizing a temperature-sensitive Rop allele

Rop-null embryos exhibited a substantial but mild cytokinesis defect without cytokinesis failure in cycle 14–16 divisions. Maternally loaded Rop likely masked a more severe cytokinesis phenotype in the *Rop*-null embryos. During oogenesis, maternal *Rop* RNA is loaded into the embryo (Tomancak et al., 2002). Although the embryo degrades a subset of maternal RNAs at the mid-blastula transition in cycle 14, low levels of Rop protein persist even in late stage $Rop^{G27}/Df(3L)GN4$ embryos (Harrison et al., 1994).

To circumvent the effect of maternally loaded Rop, we used a temperature-sensitive *Rop* mutation. Rop^{A19} and Rop^{G11} are hypomorphic point mutations (Table 1) (Harrison et al., 1994). Each allele is homozygous lethal and rescued by a Rop transgene (Harrison et al., 1994). As previously shown, both Rop^{A19} and Rop^{G11} failed to complement the null Rop^{G27} allele, but at room temperature complemented one another: $Rop^{A19/G11}$ adult males and females were viable and fertile (Table S2) (Harrison et al., 1994; Wu et al., 1998). However, at 32°C these $Rop^{A19/G11}$ adults display neurological defects and premature death, showing that the heteroallelic combination is temperature sensitive (Harrison et al., 1994).

To determine the strength of the $Rop^{A19/G11}$ mutation, we assayed embryonic viability at the permissive (25°C) and restrictive (32°C) temperatures. *Rop*-null embryos die late in embryogenesis from general secretion defects (Harrison et al., 1994). By contrast, some hypomorphic *Rop* mutants survived into larval stages (Table 1). At the permissive and restrictive temperatures, 27.0% and 0.9% of embryos from $Rop^{A19/G11}$ parents hatched (Table S3). Normal hatch rates for wild-type embryos were 87.6% at 25°C and 86.3% at 32°C, showing that the effect was specific to the $Rop^{A19/G11}$ mutation. These results suggest $Rop^{A19/G11}$ acted as a weak hypomorphic mutation at the permissive temperature and as a strong hypomorphic mutation at the restrictive temperature.

Embryonic cytokinesis requires Rop

We used the temperature-sensitive $Rop^{A19/G11}$ combination to test whether Rop was required for cytokinesis in the embryonic epithelial divisions during cycles 14–16. Mating $Rop^{A19/G11}$ females with $Rop^{A19/G11}$ males generated embryos with three different zygotic genotypes – homozygous Rop^{A19}, homozygous Rop^{G11} and heteroallelic $Rop^{A19/G11}$. Because we could not distinguish between these zygotic genotypes by genetic markers, we call the genotype of this collection of embryos Rop^{TS} (for their temperature-sensitive nature). Importantly, all three types of embryos inherited the same temperature-sensitive maternally loaded Rop protein, which made them phenotypically different from embryos with the same zygotic genotypes but maternally loaded with wild-type Rop protein from a heterozygous female parent.

Table 1. Summary of *Rop* alleles

Allele	Type of mutation[a]	Lethal stage[a]
Rop^{G27}	Null	Embryo
Rop^{A3}	Null	Embryo
Rop^{A19}	Hypomorph	Embryo to first-instar larvae
Rop^{G11}	Temperature-sensitive hypomorph	25°C, third-instar larvae 27°C, embryo
$Rop^{A19/G11}$	Temperature-sensitive	24°C, not lethal 32°C, embryo[b]

[a]According to reference (Harrison et al., 1994), unless otherwise noted.
[b]This work.

We collected wild-type and Rop^{TS} embryos and aged them at the permissive temperature until most embryos completed cellularization – a cytokinesis-like process (Fig. 4A). After shifting and aging the embryos at the restrictive temperature, we assayed for binucleate cells, the classic phenotype of failed cytokinesis. As a control, we also aged embryos for the same amount of time at the permissive temperature. Staining with anti-adducin antibody, anti-lamin antibody and DRAQ5, respectively, was used to mark the cell cortex, nuclear envelope and DNA. Both wild-type embryos at 25°C and 32°C, as well as Rop^{TS} embryos at 25°C, had low multinucleate frequencies – on average less than 3%. Rop^{TS} embryos aged at 32°C contained on average 37% binucleate and even multinucleate cells, showing that Rop was required for cytokinesis (Fig. 4B,C). Rop^{TS} embryos displayed a wide range of multinucleate frequencies, perhaps from differences between the three zygotic genotypes.

Rop^{TS} cells initiate furrow ingression normally

To determine what step of cytokinesis Rop^{TS} cells fail, we again turned to live imaging of the cycle 14 divisions, visualized by injecting fluorescent actin and histones. We used a custom-built temperature stage to incubate wild-type and Rop^{TS} embryos at 32°C prior to and during imaging. In wild-type embryos at 32°C, all cells divided normally (Fig. 5A, $n=75$ cells from six embryos; Movie 3).

Rop^{TS} cells initiated furrow ingression normally. With the exception of one cell out of 32, furrow ingression began in the Rop^{TS} cells that failed cytokinesis. Furthermore, these Rop^{TS} cells and wild-type cells initiated furrow ingression with the same timing after anaphase onset, marked by sister chromatid separation [wild type 74.8±22.7 s ($n=29$) versus Rop^{TS} 80.4±12.52 s ($n=9$); *t*-test *P*-value=0.39; mean±s.e.m.]. These results suggest that the early stages of cytokinesis, including actin-myosin ring formation and initiation of furrow ingression, are normal in Rop^{TS} cells.

Furrow regression in Rop^{TS} cells

In many Rop^{TS} cells, the cleavage furrow regressed during furrow ingression. We call this phenotype early regression (Fig. 5B,D; Movie 4). In these cells, the furrow ingressed from 30% to 75% of the cell width at the start of cytokinesis (45.9±15.9%, $n=11$; mean±s.e.m.) (Fig. 5B, second panel) but regressed before closing (Fig. 5B, right panels). Furrow ingression often proceeded slowly or stalled. The time taken from furrow ingression from initiation to regression was significantly longer in these cells compared to wild type (Fig. 5E). For example, in Fig. 5B over a minute passed between the images shown in the second and third panel with little to no ingression of the furrow. Interestingly, even some Rop^{TS} cells that divided successfully had slower furrow ingression than wild-type cells, suggesting a mild furrow ingression defect, similar to the phenotype observed in Rop^{G27} and Rop^{A3} embryos.

We also saw Rop^{TS} cells where the furrow ingressed and closed normally but then later regressed, which we call late regression (Fig. 5C). On average, this regression occurred 167±108 s after the furrow closed, but in one cell occurred 349 s – almost 6 min – after furrow closure. Because we did not film all cells for long periods after a successful furrow closure, we surely missed identifying cells

Journal of Cell Science (2016) 129, 430-443 doi:10.1242/jcs.179200

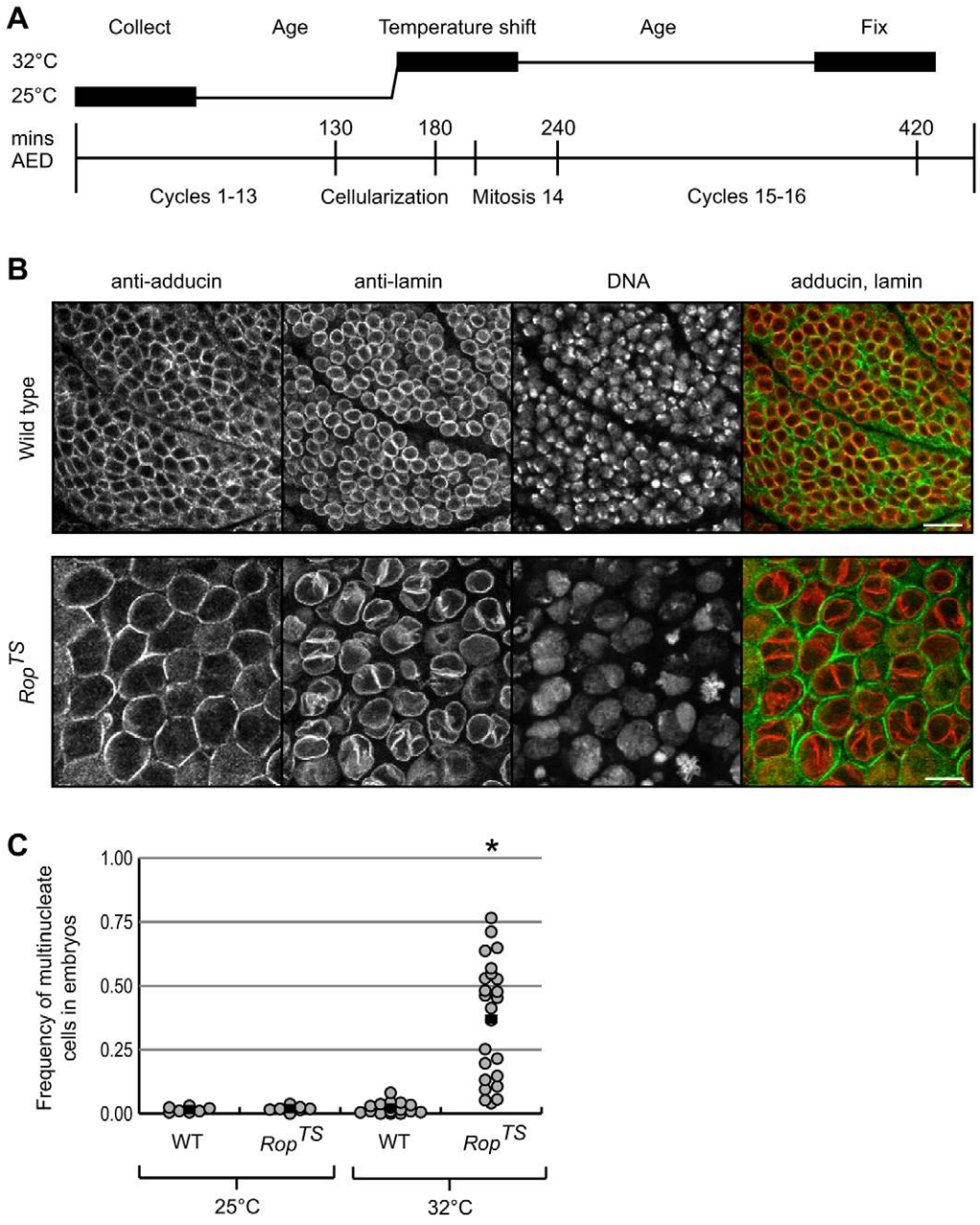

Fig. 4. Embryonic cytokinesis requires Rop. (A) Diagram of the timing of temperature shifts used in collection and aging wild-type and Rop^{TS} embryos. The bottom time line indicates the timing of mitotic cycles at 25°C in minutes after egg deposition (AED). Boxes represent the 60-min age range of embryos at collection, temperature shift and fixation. (B) Immunofluorescent images of epidermal cells of wild-type (yw^{67}) and Rop^{TS} embryos at the restrictive temperature 32°C. Antibody staining against adducin (green) and lamin (red), respectively, mark the cell membrane and nuclear envelope. DNA staining identifies mitotic cells. Scale bars: 10 µm. (C) Graph of the frequency of multinucleate cells in wild-type (WT) and Rop^{TS} embryos at the permissive (25°C) and restrictive (32°C) temperatures. Each circle represents the multinucleate frequency of one embryo. For each embryo, we scored at least 100 cells. Data from *n* embryos for each condition: WT 25°C, 7; Rop^{TS} 25°C, 7; WT 32°C, 16; Rop^{TS} 32°C, 24. Black bars indicate the average mean multinucleate frequency for each condition. *P<0.01 for Rop^{TS} embryos at 32°C compared with wild-type embryos at 25°C and 32°C degrees (*t*-test). Similar results were obtained in a second independent experiment.

in which division failed long after furrow closure. Therefore, the frequency of late regression defects compared to other failure phenotypes was likely underrepresented (Fig. 5D). Timing from initiation to completion of furrow ingression showed some cells with slower furrow ingression but that was overall not significantly different than wild-type cells (Fig. 5E).

Maintenance of the contractile ring and central spindle requires Rop

To further investigate the early regression phenotype in Rop^{TS} cells, we performed live imaging of embryos with a GFP-tagged Spaghetti squash fusion protein (Royou et al., 2004). In *Drosophila*, *spaghetti squash* (*sqh*) encodes the regulatory light chain for non-muscle myosin II (Karess et al., 1991). In previous experiments, we focused on cells that divided parallel to the *x-y* plane, creating a cross-sectional view of the daughter cells and ingressing cleavage furrow. In this experiment, we found that when a cell divides perpendicular to the *x-y* plane, the maximum projection of three *z*-planes gave an informative top-down view of the circular contractile ring (Fig. 6A).

In wild-type cells, the contractile ring formed and contracted until closed (n=37 cells from three embryos) (Fig. 6A). Recapitulating our previous results, all Rop^{TS} cells that failed cytokinesis initiated furrow ingression normally (n=23 from four embryos) and some cells failed cytokinesis by early regression (n=15 from four embryos). In these cells, myosin localized normally to the cleavage furrow. Furrow ingression, indicated by the decreasing diameter of the contractile ring, progressed, on average, to one-third the original width of the cleavage furrow (32.3±20.0%, n=9; mean± s.e.m.). Then, a gap formed in the myosin II ring. Over time this gap expanded as the ring disassembled, until only a small remnant remained (Fig. 6A, arrowheads) (n=11 from four embryos). These results indicate that a failure to maintain the contractile ring during ingression causes the early regression phenotype in Rop^{TS} cells.

Journal of Cell Science (2016) 129, 430-443 doi:10.1242/jcs.179200

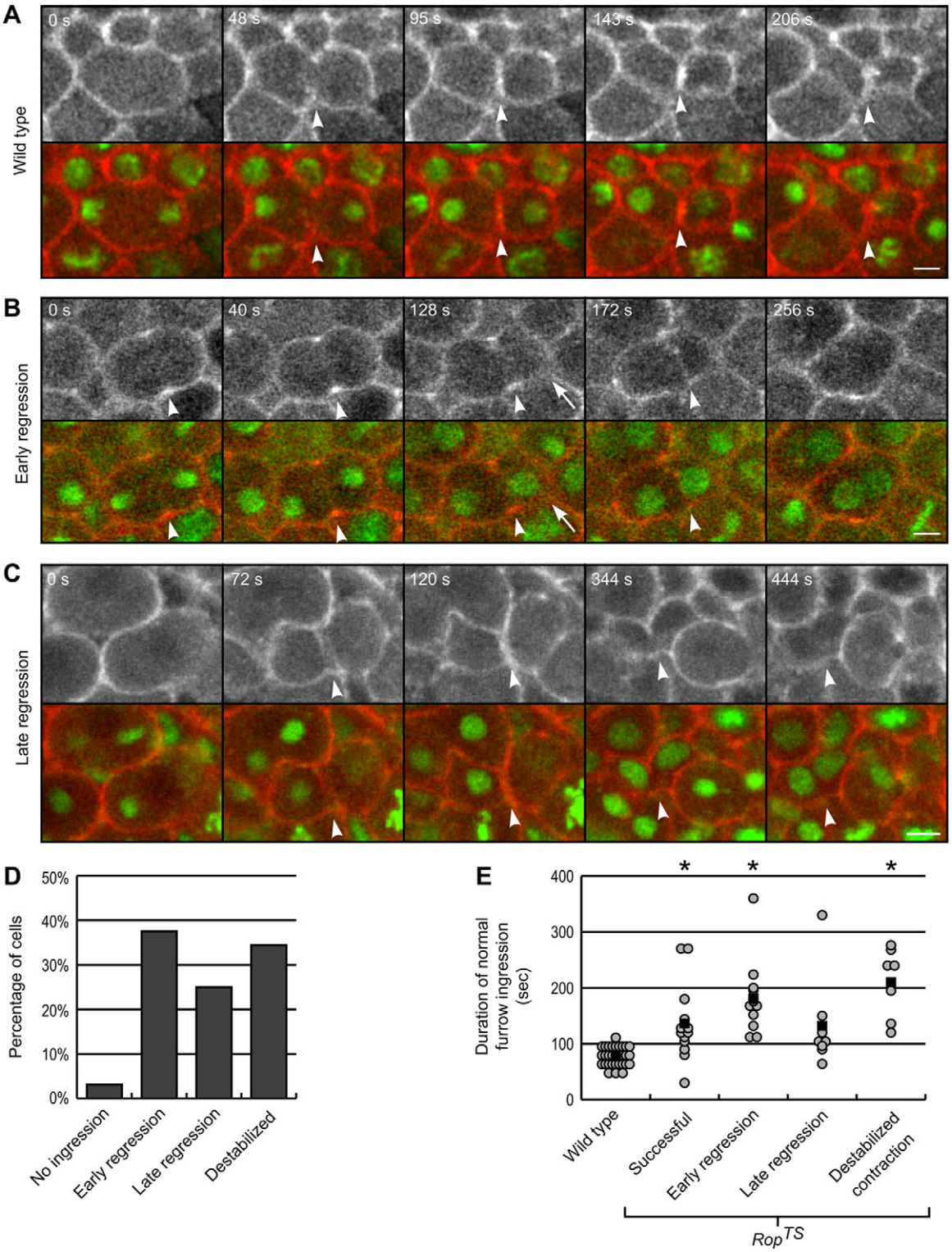

Fig. 5. Furrow regression during cytokinesis in *Rop*^{TS} embryos. (A–C) Time-lapse images of cytokinesis in (A) wild-type (*yw*^{67}) and (B,C) *Rop*^{TS} embryos at the restrictive temperature 32°C. Rhodamine–actin (gray or red) labels the cell cortex and Cy5–histone (green) marks DNA. The time after initiation of furrow ingression is denoted in the upper-left corner. Arrowheads follow the cleavage furrow. (A, Movie 3) Example of normal furrow ingression in wild-type cell. (B, Movie 4) Example of an early regression cytokinesis failure. Furrow ingression began but stalled and regressed before ingression completed. Abnormal cell shape also observed (arrow). (C) Example of a late regression cytokinesis failure. Furrow ingression proceeded normally through completion but then later regressed. Scale bars: 5 µm. (D) Bar graph of the frequency of the type of cytokinesis failure in *Rop*^{TS} cells. *n*=32 failed divisions from seven embryos. (E) Graph of the duration of furrow ingression in wild-type and *Rop*^{TS} cells at 32°C. For wild-type and successful and late regression *Rop*^{TS} cells, furrow ingression was measured from initiation to completion. For *Rop*^{TS} cells exhibiting the early regression phenotype, furrow ingression timing was measured from furrow initiation to the onset of regression. For *Rop*^{TS} cells exhibiting the destabilized contraction phenotype, furrow ingression timing was measured from furrow initiation to destabilization, defined as a nucleus moving through the contractile ring. Data from *n* cells for each condition: wild type, 31; successful, 14; early regression, 12; late regression, 8; destabilized contraction, 7. **P*<0.01 from wild-type (*t*-test).

Journal of Cell Science (2016) 129, 430-443 doi:10.1242/jcs.179200

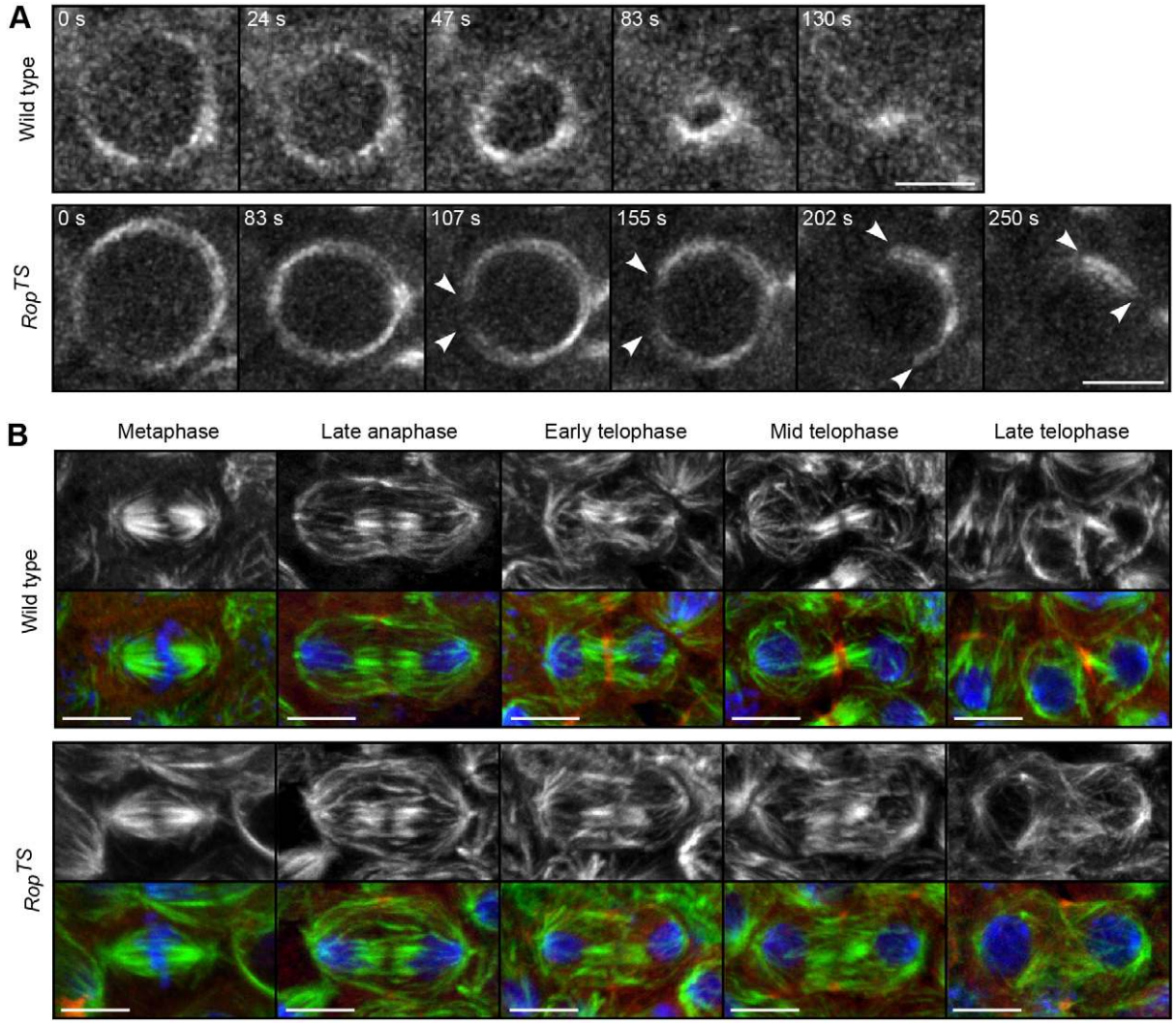

Fig. 6. Disassembly of contractile ring causes early regression in *Rop*^{TS} cells. (A) Time-lapse images of contractile ring marked by the myosin regulatory light chain fused to GFP (Sqh–GFP) in wild-type and *Rop*^{TS} cells at 32°C. Imaging cells that divided perpendicular to the *x-y* plane produced an end-on view of the contractile ring. Arrowheads follow the gap in the ring as it disassembled. A maximum projection of three *z*-planes is shown. Time from initiation of furrow ingression indicated. (B) Immunofluorescent images of dividing epithelial cells in wild-type (*yw*^{67}) and *Rop*^{TS} embryos at 32°C. Anti-tubulin staining (gray or green) shows *Rop*^{TS} cells have normal microtubules metaphase through early telophase. By late telophase, identified by decondensed nuclei, central spindle microtubules became disorganized and less dense. Anti-anillin antibody (red) and DRAQ5 (blue) staining, respectively, mark the contractile ring and DNA. Maximum projection of multiple *z*-planes. *n* cells were analyzed for each stage: wild type, 46, 38, 9, 16 and 18; *Rop*^{TS}, 34, 34, 8, 24 and 34. Representative images are shown. Scale bars: 5 µm.

In these experiments, we also injected embryos with fluorescently labeled tubulin to monitor cell division. As expected, upon cytokinesis in wild-type cells the microtubules first bundled into a central spindle and then compressed into a midbody as the cleavage furrow ingressed (Fig. S2A; Movie 5) (n=36/37 cells from three embryos). In *Rop*^{TS} cells at 32°C, we observed normal mitotic spindles (Fig. S2B, left panel; Movie 6) (n=13/13 cells from three embryos), consistent with the normal chromosome segregation during mitosis observed in the previous experiment (H.D., unpublished observation). These results show that the cytokinesis defects in *Rop*^{TS} cells did not arise from gross defects in spindle assembly and dynamics. During telophase, microtubules bundled into a central spindle (Fig. S2B, arrow) but never formed a midbody when ingression failed (n=12/12 cells from four embyros). Instead, microtubules disappeared from the central midzone immediately prior to gap formation in the contractile ring (Movie 6).

We confirmed these results by staining for tubulin and DNA in wild-type and *Rop*^{TS} embryos aged at the restrictive temperature (Fig. 6B). In analysis of fixed cells, the fate of a cell in cytokinesis is unknown. Therefore, we only analyzed cells from embryos with high binucleate frequencies, increasing the likelihood that these cells would have also failed cytokinesis. Tubulin staining showed normal mitotic spindles, including astral and furrow microtubules, in wild-type (n=46) and *Rop*^{TS} cells (n=34). During anaphase and early telophase the central spindle microtubules bundled together properly (wild type n=47 cells; *Rop*^{TS} n=42 cells). However, in late telophase, the central spindle microtubules became disorganized in the majority of *Rop*^{TS} cells (n=34). Staining for anillin, a contractile ring protein, also showed its normal localization at the cleavage furrow in *Rop*^{TS} cells (Fig. 6B).

Cell shape instability during cytokinesis in *Rop*^{TS} cells

In addition to the classic furrow regression phenotypes in *Rop*^{TS} cells, we unexpectedly observed a third type of cytokinesis failure, which we call destabilized contraction (Figs 5D and 7A; Movie 7). In these *Rop*^{TS} cells, a central cleavage furrow

Journal of Cell Science (2016) 129, 430-443 doi:10.1242/jcs.179200

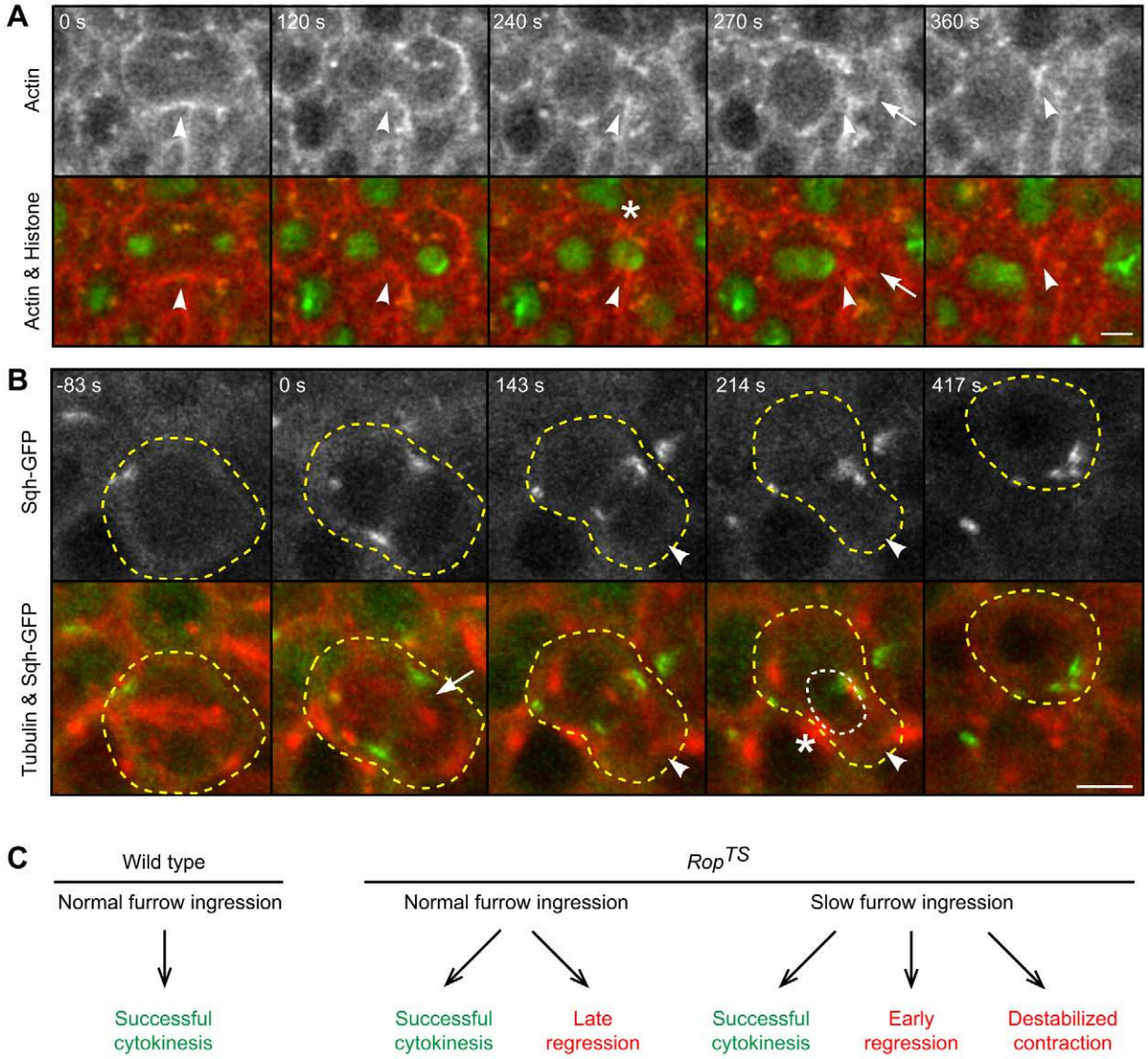

Fig. 7. Unstable cell shape during cytokinesis in *Rop*^{TS} cells. (A) Destabilized contraction in a *Rop*^{TS} cell. Rhodamine–actin (gray or red) labels the cell cortex and Cy5–histone (green) marks DNA. Arrowheads follow the cleavage furrow. Furrow ingression began but stalled. One daughter nucleus moved through the contractile ring (asterisk) as that daughter cell shrunk in size. Furrow closure pinched off a small anucleate cell (arrow). The time since initiation of furrow ingression is shown. Results correspond to Movie 7. (B) Time-lapse images of destabilized contraction in *Rop*^{TS} cells at 32°C. The myosin regulatory light chain fused to GFP (Sqh–GFP, green) marks the contractile ring. No ectopic myosin present in cell cortex outside furrow (arrowhead). HiLyte-647-conjugated tubulin (red) labels microtubules. Midzone microtubules formed normally (arrow). Yellow dashed lines indicate the approximate cell boundary. The white dashed line outlines the daughter nucleus as it moves through the contractile ring. The time from the initiation of furrow ingression is indicated in upper-left corner. A maximum projection of two *z*-planes is shown. (C) Summary of cytokinesis phenotypes observed in wild-type and *Rop*^{TS} cells at the restrictive temperature. Scale bars: 5 µm.

formed properly and furrow ingression again proceeded slowly (Figs 5E and 7A). Then, during furrow ingression, cell shape became unstable such that one daughter cell shrunk in size as the other daughter cell enlarged (Fig. 7A; Movie 7). This change in cell shape was accompanied by one daughter nucleus rapidly moving through the contractile ring, which had ingressed about half way (63.0±9.4%, n=7 cells; mean±s.e.m.). Finally, completion of furrow ingression led to the formation of a binucleate cell and a tiny anucleate cell (Fig. 7A, arrow). During these shape changes, the contractile ring did not move relative to neighboring cells, suggesting that the phenotype was not caused by ring detachment or ring slippage. We also observed mild cell shape instabilities where daughter cells transiently differed in size in seven of the 12 cells that had failed cytokinesis by early regression (Fig. 5B, arrow). In these cases, though, no nuclear movement occurred.

Similar cell shape instabilities during cytokinesis have been previously documented in tissue culture cells with reduced expression of the actin-binding proteins anillin, profilin, diaphanous or supervillin (Dean et al., 2005; Straight et al., 2005; Hickson and O'Farrell, 2008; Piekny and Glotzer, 2008; Smith et al., 2010; Sedzinski et al., 2011). In these cases, mislocalization of myosin II from the cleavage furrow to the cell cortex caused ectopic polar contractions and rapid oscillations in daughter cell shape and size. However, in the destabilized *Rop*^{TS} cells, myosin localized to and remained at the cleavage furrow without mislocalization to the cell cortex of the shrinking daughter cell (Fig. 7B, arrowhead) (n=8 from three embryos). In addition,

Journal of Cell Science (2016) 129, 430-443 doi:10.1242/jcs.179200

staining wild-type and Rop^{TS} embryos aged at the restrictive temperature showed that these cells also had normal cortical F-actin during cytokinesis (Fig. S3). Thus, unlike for the genes analyzed in previous reports, the cell shape instability in Rop^{TS} cells was not driven by ectopic actin-myosin contractions at the polar cortex.

DISCUSSION

Cytokinesis requires the Sec1/Munc18 protein Rop

Our data demonstrate that furrow ingression and abscission during cytokinesis requires Rop, a Sec1/Munc18 protein that mediates exocytosis. This adds to a growing literature concluding that furrow ingression during cytokinesis often involves both contraction of an actin-myosin ring and vesicle-mediated membrane addition (Albertson et al., 2005; McKay and Burgess, 2011). Mutations in the t-SNARE syntaxin also cause defects in furrow ingression and abscission, showing that trans-SNARE complexes mediate membrane fusion at the cleavage furrow (Burgess et al., 1997; Jantsch-Plunger and Glotzer, 1999; Somma et al., 2002; Low et al., 2003). By interacting with syntaxin, Sec1/Munc18 proteins regulate the assembly and activity of the trans-SNARE complex (Carr and Rizo, 2010). Our results suggest that Rop regulates syntaxin-mediated vesicle fusion during cytokinesis.

Using live imaging, we discovered slowed furrow ingression in *Rop*-null embryos (Fig. 3). We hypothesize this is a direct consequence of reduced Rop-mediated vesicle addition to the ingressing furrow. If actin-myosin contraction outpaces membrane growth, the plasma membrane might rupture from insufficient surface area (Danilchik et al., 1998; Field et al., 2005). Thus, the integrity of the advancing furrow requires coordinating contraction with membrane addition. The slowed furrow ingression in *Rop*-null embryos implies that a feedback mechanism might slow actin-myosin contraction to compensate for reduced membrane growth.

Maternally loaded Rop likely compensated partially for the *Rop*-null mutation, masking a more severe phenotype (Baker et al., 1982; Langley et al., 2014). To bypass maternal loading, we used a temperature-sensitive *Rop* mutant. Rop^{TS} embryos aged at the restrictive temperature contained many binucleate cells, indicative of failed cytokinesis (Fig. 4). This is consistent with the binucleate phenotype observed after knockdown of Rop in an RNAi screen in *Drosophila* S2 cells (Echard et al., 2004).

We further used live imaging to determine the cause of cytokinesis failure in Rop^{TS} cells. Furrow ingression initiated normally, suggesting that Rop-mediated vesicle fusion was not required for establishing the site of the cleavage furrow or assembling the contractile ring. Consistently, both the myosin regulatory light chain (Sqh–GFP) and anillin localized properly to the cleavage furrow (Fig. 6). We observed multiple cytokinesis defects in Rop^{TS} cells (Fig. 7C). In some Rop^{TS} cells, furrows ingressed with normal kinetics. These cells either successfully completed cytokinesis, or failed abscission and regressed. In the remaining Rop^{TS} cells, furrows ingressed slowly and often stalled. These cells successfully completed cytokinesis, regressed during furrow ingression or lost cell shape stability (Fig. 7C).

Maintenance of the contractile ring requires Rop-mediated vesicle addition

In Rop^{TS} cells exhibiting early regression, the contractile ring disassembled (Fig. 6A). Previous studies have demonstrated a similar connection between vesicle addition and contractile ring integrity during furrow ingression (Giansanti et al., 2004, 2006, 2007; VerPlank and Li, 2005; Gatt and Glover, 2006; Robinett et al., 2009), perhaps because vesicles deliver both actin and actin remodelers, as well as membrane, to the cleavage furrow during cytokinesis (Albertson et al., 2008; Cao et al., 2008; Dambournet et al., 2011; Schiel et al., 2012). Therefore, we propose that disruption of the Rop-mediated vesicle fusion at the advancing furrow also disrupts actin regulation at the cleavage furrow in Rop^{TS} cells, causing ring disassembly and furrow regression.

An alternative explanation for ring disassembly is that furrow ingression is so slow that the cell progressed into interphase before completing cytokinesis. The time period in which a cell is competent to execute cytokinesis is known as C-phase (Martineau et al., 1995; Canman et al., 2000). It was possible that exiting C-phase before finishing cytokinesis causes furrow regression in Rop^{TS} cells. This model predicts a temporal cutoff in cytokinesis, with any cell failing cytokinesis if it delays too long after anaphase onset. Our timing analysis of furrow ingression suggests that this is not the case for Rop^{TS} cells. Some Rop^{TS} cells slowly but successfully completed furrow ingression 250 s after initiating ingression. Thus, the many cells that underwent regression before 250 s after initiation were likely still in C-phase.

We also observed disorganized central spindles in Rop^{TS} cells with early regression (Fig. 6B, Fig. S2, Movie 6); however, timing suggests that the primary defect is in furrow ingression. At the onset of cytokinesis, furrows ingressed slowly, whereas the central spindle always formed and bundled properly, only later disappearing or becoming disorganized. Maintenance of the central midzone and the contractile ring requires signaling between the two structures (Martineau et al., 1995; Carmena et al., 1998; Giansanti et al., 1998; Gatti et al., 2000; Somma et al., 2002; Straight et al., 2003). We hypothesize that as Rop^{TS} cells lose contractile ring integrity, signals to maintain the central spindle are also lost.

Cell shape stability during cytokinesis requires Rop

We also observed cell shape instability in Rop^{TS} cells at the restrictive temperature. During cytokinesis, daughter cells changed size where one daughter cell increased in size as the other cell decreased in size. This phenotype was either mild and transient, as observed in early regression cells (Fig. 5B, arrow), or extreme, as observed upon destabilized contraction (Fig. 7; Movie 7). Researchers have previously observed such instability in cell shape during cytokinesis in cell culture experiments (Dean et al., 2005; Straight et al., 2005; Hickson and O'Farrell, 2008; Piekny and Glotzer, 2008; Smith et al., 2010; Sedzinski et al., 2011). To our knowledge, the studies presented here are the first report of cell shape instabilities during cytokinesis within an epithelial tissue.

During cytokinesis, an imbalance in polar cortical forces or a global increase in cortical tension can cause cell shape instability (Sedzinski et al., 2011). What force drives the destabilized contraction in Rop^{TS} cells remains unclear. Unlike previously reported examples, myosin did not mislocalize to the contracting polar cortex of Rop^{TS} cells (Fig. 7B). Although Munc18-1 regulates actin depolymerization at the cell cortex in mammalian cells (Toonen et al., 2006), Rop^{TS} cells displayed normal cortical actin during cytokinesis (Fig. S3). Furthermore, during cycle 14 divisions in *Drosophila* embryos, other cytokinesis mutants with slow furrow ingression, such as *Df(3R)Exel7283* and *Cyclin B3*, maintained a stable cell shape (Echard and O'Farrell, 2003). This shows that external forces from neighboring cells are insufficient to destabilize a slowly dividing cell. Whatever the force, we hypothesize that the increasing pressure from the shrinking daughter cell pushes the daughter nucleus through the contractile ring because nuclear movement always coincided with the change in cell size.

Journal of Cell Science (2016) 129, 430-443 doi:10.1242/jcs.179200

Rop and syntaxin function together during cytokinesis

During vesicle fusion, Sec1/Munc18 proteins regulate the assembly and activity of trans-SNARE complexes by interacting with the t-SNARE syntaxin. We found that Rop is required for furrow ingression and abscission – the same steps in cytokinesis that require syntaxin (Jantsch-Plunger and Glotzer, 1999; Somma et al., 2002; Low et al., 2003). This suggests that Rop and syntaxin function together during cytokinesis.

We interpret the *Rop* mutant cytokinesis phenotype as a consequence of decreased vesicle fusion at the cleavage furrow. However, we should note that, in *Drosophila* Rop both inhibits and promotes vesicle fusion at the neuronal synapse (Schulze et al., 1994; Wu et al., 1998). Two viable mutations in *Rop* disrupt its inhibitory role and increase neurotransmitter release (Wu et al., 1998). Because cytokinesis is an essential process, this suggests that the inhibitory function of Rop is not essential to its role in cytokinesis. Rop^{A19} and Rop^{G11} – the two mutations used in this study for the temperature-sensitive combination – decrease neurotransmitter release (Harrison et al., 1994; Wu et al., 1998). This suggests that Rop functions in cytokinesis by promoting vesicle fusion, consistent with the similar phenotypes between syntaxin and Rop.

A Sec1/Munc18 protein and syntaxin also function together during plant cytokinesis (Assaad et al., 1996, 2001; Waizenegger et al., 2000). Restricted by their rigid cell walls, during cell division plant cells build a new cell membrane from within by fusion of Golgi-derived vesicles (Jürgens, 2005). The Sec1/Munc18 homolog KEULE stabilizes the open confirmation of its syntaxin KNOLLE to promote formation of trans-SNARE complexes between vesicles at the cell plate (Park et al., 2012). Taken together with our results, this highlights conserved functions of vesicle trafficking genes between plant and animal cytokinesis.

A live-imaging screen for cytokinesis defects in the *Drosophila* embryo

Using live imaging of *Drosophila* embryos, we also screened deficiencies for defects in cytokinesis. We identified three deficiencies with cytokinesis phenotypes (Fig. 2C). Importantly, live imaging detected subtle phenotypes, such as slow furrow ingression and ectopic blebbing, that did not cause cytokinesis failure and would be missed by a fixed single-time point analysis.

Df(3L)R-G5 embryos exhibited increased blebbing during cytokinesis. Although blebs at the cell poles commonly occur during cytokinesis (Charras, 2008), *Df(3L)R-G5* cells exhibited a higher frequency of polar blebs. These polar blebs release cortical tension to stabilize cell shape during cytokinesis (Sedzinski et al., 2011). Large membrane blebs also occurred at the cleavage furrow in two cells in a *Df(3L)R-G5* embryo (Fig. 2E). Such equatorial membrane blebs do not normally occur during cytokinesis. Researchers previously observed similar membrane blebs at the cleavage furrow in the absence of anillin, a contractile ring protein that cross-links the actin-myosin ring to the membrane (Somma et al., 2002; Echard et al., 2004). Although the *Df(3L)R-G5* genomic region does not include anillin, it might encode a protein that regulates forces at the cell cortex or mediates cytoskeletal attachment to the plasma membrane.

We based the logic of our deficiency screen on a strategy developed by Wieschaus and colleagues (Merrill et al., 1988). In *Drosophila*, the 13 syncytial divisions before cellularization do not require zygotic gene expression. Through deficiency screening of the entire genome, Wieschaus and colleagues showed that only seven zygotic genes were required for cellularization (Merrill et al., 1988; Wieschaus and Sweeton, 1988). Because the first conventional cytokinesis in *Drosophila* embryos immediately follows cellularization, we used the same approach to begin screening the zygotic genome for genes required for cytokinesis. By screening 15% of the third chromosome, we identified three genomic regions. This suggests the remainder of the genome will yield many more zygotic genes important in cytokinesis. Finally, we point out that this same logic can be used to identify zygotically expressed genes that are required in other cellular and developmental events that occur immediately following cellularization, such as gastrulation and germ band elongation.

MATERIALS AND METHODS

Fly strains and husbandry

We used the following *Drosophila melanogaster* fly strains: TM3, *twist-GAL4,UAS-GFP* and FM7c, *twist-GAL4,UAS-GFP* balancer chromosomes (Halfon et al., 2002); *UAS-Synaptotagmin-GFP* (UAS-Syt-GFP) (Zhang et al., 2002); *matα-GAL4-VP16* driver; $nullo^{6F1-2}$ (Wieschaus and Sweeton, 1988); EMS-induced mutations Rop^{G27}, Rop^{A3}, Rop^{A19} and Rop^{G11} (Harrison et al., 1994); *spaghetti squash-GFP* (Royou et al., 2004); and y,w^{67} for wild type. Table S1 lists the deficiency lines screened for cytokinesis defects. Flies were raised on standard cornmeal and molasses food at room temperature (18–21°C) or 25°C. The $Rop^{A19/G11}$ flies must be raised at room temperature. Embryos were collected on grape agar plates from collection bottles, as previously described (Rothwell and Sullivan, 2000).

Screen for cytokinesis defects

To screen for cytokinesis defects in mutant cycle 14 embryos, we performed a two-generation crossing scheme. *matα-GAL4-VP16*, *UAS-Syt-GFP*; *Dr*/Tm3, *twist-GAL4, UAS-GFP* crossed to *Df*/balancer produced *matα-GAL4-VP16*, *UAS-Syt-GFP*/+; *Df*/Tm3, *twist-GAL4, UAS-GFP* females that were then crossed to *Df*/Tm3, *twist-GAL4, UAS-GFP* males. Embryos were collected from this second cross and homozygous deficiency embryos were identified by the absence of the TM3, *twist-GAL4,UAS-GFP* balancer chromosome, which gives GFP fluorescence in the mesoderm by stage 8 of embryogenesis (Halfon et al., 2002). For deficiencies on the X chromosome, a similar crossing scheme with the FM7c *twist-GAL4, UAS-GFP* balancer chromosome was used. At least two homozygous mutant embryos were analyzed for each deficiency line.

Live embryo analysis

To image live embryos, embryos were collected for 1 h and then aged at 25°C for 75 min for embryos being injected or for 3 h for Syt–GFP embryos. Embryos were then hand-dechorionated on double-sided tape, affixed to the cover glass slide by heptane-based glue, desiccated for 8–10 min, if being injected, and covered in halocarbon oil (Tram et al., 2001).

Embryos were injected with fluorescently labeled proteins as previously described, except needles were loaded from the front instead of the back (Tram et al., 2001). Briefly, protein was injected at approximately one-third length of the embryos from the anterior pole during syncytial cycles 12–13 or cellularization. We used Rhodamine-labeled non-muscle actin (catalog number APHR, Cytoskeleton, Inc.; Denver, CO) reconstituted in general actin buffer (5 mM Tris-HCl pH 8.0, 0.2 mM $CaCl_2$, 0.2 mM ATP and 0.1 mM DTT) at 2 or 3.3 mg/ml for single injection experiments, and 5 mg/ml for double injection experiments. We injected HiLyte-Fluor-647-labeled tubulin (catalog number TL670M, Cytoskeleton, Inc.) at 10 mg/ml, reconstituted in general tubulin buffer (catalog number BST01, Cytoskeleton, Inc.). Cy5-labeled histones H2A and H2B were kindly provided by Ellen Homola (University of Alberta, Canada). Embyros were not used for imaging if they showed extensive trauma from injection, such as severe nuclear fallout or excessive bleeding of cytoplasm at the site of injection. Injection experiments were repeated over multiple days and the data pooled together.

When required, embryos were shifted to 32°C during cellularization using a custom-built temperature stage that heated the halocarbon oil through a surrounding temperature-controlled metal plate. Slides were glued to this

metal plate using heat paste, and the temperature of the halocarbon oil was monitored with a thermocouple thermometer (catalog number HH506RA, Omega, Stamford, CT). When turned on, the temperature stage elevated the halocarbon oil from room temperature to 32°C within 1 min. Afterwards, the halocarbon oil temperature fluctuated by one degree, centered around 32°C. Images were acquired using a dry objective to avoid the heat sink of an oil objective.

Embryo fixation and immunostaining

Embryos were collected, fixed by the fast formaldehyde fix protocol and stained as previously described with the few noted differences (Rothwell and Sullivan, 2000). Briefly, embryos were dechorionated by treating with a 50% bleach solution for 1–2 min. Embryos were fixed for 5 min with 37% formaldehyde, and the vitelline membrane was cracked with methanol. Embryos were incubated in methanol overnight at 4°C to clear out yolk. Embryos were directly rehydrated in PBS, 0.5% BSA and 0.1% Triton X-100 for 15 min. When staining with phalloidin for F-actin, embryos were devitellinized by hand instead of with methanol, as previously described (Rothwell and Sullivan, 2000).

Primary and secondary antibodies were incubated at room temperature in PBS, 5% BSA, 0.1% Triton X-100 for 4 h or 1–2 h, respectively. We used the antibodies 1B1 mouse anti-adducin at 1:10 (Developmental Studies Hybridoma Bank, Iowa City, Iowa, USA), rabbit anti-lamin at 1:2000 (Lin and Fisher, 1990), 4F8 mouse anti-Rop at 1:10 (Developmental Studies Hybridoma Bank), mouse anti-α-tubulin at 1:100 (catalog number T9026, Sigma, St Louis, MO), Rhodamine-labeled rabbit anti-anillin at 1:200 (Field and Alberts, 1995) and Alexa-Fluor-488- and -546-conjugated goat secondary antibodies at 1:600 (Molecular Probes, Inc. by Thermo Fisher Scientific, Waltham, MA). To visualize F-actin, Alexa-Fluor-488–phalloidin (catalog number A12379, Molecular Probes, Inc.) was added at 1:100 during staining with the secondary antibodies. To stain DNA, embryos were incubated with 6.66 µM DRAQ5 (ab108410, Abcam, Cambridge, UK) for 1 h at room temperature and washed overnight at 4°C. Embryos were mounted in a glycerol-based mounting medium.

Microscopy, image processing, image analysis and statistics

Images were acquired at room temperature on a Leica Microsystems (Wetzlar, Germany) SP2 scanning laser confocal microscope with an inverted photoscope (Leitz DMIRB) using Leica Confocal Software (v2.61). We used the following objective lenses with the corresponding cover slide: 63× HCX PL APO 1.4 NA oil objective (No. 1 to 1.5 cover glass), 40×0.6 CORR PH2 dry objective (1 mm glass slide) and 40× HCX PL FLUOTAR 0.75 NA dry objective (No. 1.5 cover glass).

Using Fiji (ImageJ) and Adobe Photoshop, all images were adjusted to increase brightness and scaled without interpolation. Time-lapse images of live samples were filtered with a Gaussian blur ($\sigma \leq 1$ pixel). Membrane blebbing, furrow ingression timing and multinucleate frequency were determined manually in Fiji, in the last case using the 'Cell Counter' plug-in. For consistency in the analysis of membrane blebs, we only analyzed cells surrounded by neighboring cells. Data were randomly blinded for analysis of multinucleate frequency presented in Fig. 4 and for analysis of furrow ingression timing presented in Fig. 3.

n was defined as the number of cells analyzed and statistical analyses were only performed when three or more embryos were analyzed per genotype. Two-tailed Student's *t*-tests were performed assuming unequal variance when an F-test showed significantly different variances between samples. To compensate for multiple comparisons, a Bonferonni correction was used and *P* values considered significant when less than 0.01.

Egg hatch analysis

Embryos were collected on grape plates for 1 h at 25°C. Yeast paste, applied to the grape plate prior to collection to encourage egg laying, was removed from the plates before shifting them to 32°C because the yeast spreads when incubated at 32°C for long time periods. Grape plates and embryos were shifted to 32°C and aged for 30 h. Afterwards, we scored the number of hatched and unhatched embryos on the plate. Three biological replicates were performed and the mean±s.d. egg hatch frequency reported.

Acknowledgements

We thank Hugo Bellen for providing the Rop^{A19} and Rop^{G11} fly lines and the anti-Rop antibody, Paul Fisher for the anti-lamin antibody and Ellen Homola for the Cy5-conjugated histones. We offer our deepest gratitude to Michael Mason for building a custom temperature stage for our confocal microscope. We also thank Ben Abrams for his help with microscopy and the use of the dry objectives. We thank members of the Sullivan laboratory for helpful discussions about this project and manuscript.

Competing interests

The authors declare no competing or financial interests.

Author contributions

W.S. conceived and designed the deficiency screen and Rop-related experiments. R.A. designed, conducted and analyzed the deficiency and candidate screens. H.D. and Z.S. designed, performed and analyzed experiments to characterize the role of Rop in cytokinesis. H.D., Z.S. and W.S. wrote the paper.

Funding

This work was funded by the National Institutes of Health 5 [grant number R01 GM046409 to W.S.]; the National Institutes of Health Postdoctoral Individual National Research Service Award 5 [grant number F32 GM075670 to R.A.]; and a Faculty Development Grant from Albion College for R.A. Deposited in PMC for release after 12 months.

Supplementary information

Supplementary information available online at
http://jcs.biologists.org/lookup/suppl/doi:10.1242/jcs.179200/-/DC1

References

Albertson, R., Riggs, B. and Sullivan, W. (2005). Membrane traffic: a driving force in cytokinesis. *Trends Cell Biol.* **15**, 92-101.

Albertson, R., Cao, J., Hsieh, T.-s. and Sullivan, W. (2008). Vesicles and actin are targeted to the cleavage furrow via furrow microtubules and the central spindle. *J. Cell Biol.* **181**, 777-790.

Assaad, F. F., Mayer, U., Wanner, G. and Jürgens, G. (1996). The KEULE gene is involved in cytokinesis in Arabidopsis. *Mol. Gen. Genet.* **253**, 267-277.

Assaad, F. F., Huet, Y., Mayer, U. and Jürgens, G. (2001). The cytokinesis gene KEULE encodes a Sec1 protein that binds the syntaxin KNOLLE. *J. Cell Biol.* **152**, 531-544.

Baker, B. S., Smith, D. A. and Gatti, M. (1982). Region-specific effects on chromosome integrity of mutations at essential loci in Drosophila melanogaster. *Proc. Natl. Acad. Sci. USA* **79**, 1205-1209.

Burgess, R. W., Deitcher, D. L. and Schwarz, T. L. (1997). The synaptic protein syntaxin1 is required for cellularization of Drosophila embryos. *J. Cell Biol.* **138**, 861-875.

Canman, J. C., Hoffman, D. B. and Salmon, E. D. (2000). The role of pre- and post-anaphase microtubules in the cytokinesis phase of the cell cycle. *Curr. Biol.* **10**, 611-614.

Cao, J., Albertson, R., Riggs, B., Field, C. M. and Sullivan, W. (2008). Nuf, a Rab11 effector, maintains cytokinetic furrow integrity by promoting local actin polymerization. *J. Cell Biol.* **182**, 301-313.

Carmena, M., Riparbelli, M. G., Minestrini, G., Tavares, A. M., Adams, R., Callaini, G. and Glover, D. M. (1998). Drosophila polo kinase is required for cytokinesis. *J. Cell Biol.* **143**, 659-671.

Carr, C. M. and Rizo, J. (2010). At the junction of SNARE and SM protein function. *Curr. Opin. Cell Biol.* **22**, 488-495.

Charras, G. T. (2008). A short history of blebbing. *J. Microsc.* **231**, 466-478.

Dambournet, D., Machicoane, M., Chesneau, L., Sachse, M., Rocancourt, M., El Marjou, A., Formstecher, E., Salomon, R., Goud, B. and Echard, A. (2011). Rab35 GTPase and OCRL phosphatase remodel lipids and F-actin for successful cytokinesis. *Nat. Cell Biol.* **13**, 981-988.

Danilchik, M. V., Funk, W. C., Brown, E. E. and Larkin, K. (1998). Requirement for microtubules in new membrane formation during cytokinesis of Xenopus embryos. *Dev. Biol.* **194**, 47-60.

Danilchik, M. V., Bedrick, S. D., Brown, E. E. and Ray, K. (2003). Furrow microtubules and localized exocytosis in cleaving Xenopus laevis embryos. *J. Cell Sci.* **116**, 273-283.

Dean, S. O., Rogers, S. L., Stuurman, N., Vale, R. D. and Spudich, J. A. (2005). Distinct pathways control recruitment and maintenance of myosin II at the cleavage furrow during cytokinesis. *Proc. Natl. Acad. Sci. USA* **102**, 13473-13478.

Echard, A. and O'Farrell, P. H. (2003). The degradation of two mitotic cyclins contributes to the timing of cytokinesis. *Curr. Biol.* **13**, 373-383.

Echard, A., Hickson, G. R. X., Foley, E. and O'Farrell, P. H. (2004). Terminal cytokinesis events uncovered after an RNAi screen. *Curr. Biol.* **14**, 1685-1693.

Eggert, U. S., Kiger, A. A., Richter, C., Perlman, Z. E., Perrimon, N., Mitchison, T. J. and Field, C. M. (2004). Parallel chemical genetic and genome-wide RNAi screens identify cytokinesis inhibitors and targets. *PLoS Biol.* **2**, e379.

Eggert, U. S., Mitchison, T. J. and Field, C. M. (2006). Animal cytokinesis: from parts list to mechanisms. *Annu. Rev. Biochem.* **75**, 543-566.
Field, C. M. and Alberts, B. M. (1995). Anillin, a contractile ring protein that cycles from the nucleus to the cell cortex. *J. Cell Biol.* **131**, 165-178.
Field, C. M., Coughlin, M., Doberstein, S., Marty, T. and Sullivan, W. (2005). Characterization of anillin mutants reveals essential roles in septin localization and plasma membrane integrity. *Development* **132**, 2849-2860.
Foe, V. E. (1989). Mitotic domains reveal early commitment of cells in Drosophila embryos. *Development* **5**, 322.
Foe, V. E. and Alberts, B. M. (1983). Studies of nuclear and cytoplasmic behaviour during the five mitotic cycles that precede gastrulation in Drosophila embryogenesis. *J. Cell Sci.* **61**, 31-70.
Foe, V. E., Odell, G. M. Edgar, B. A. (1993). Mitosis and morphogenesis in the Drosophilan embryo: point and counterpoint. In *The Development of Drosophila Melanogaster* (ed. M. Bate and A. M. Arias), pp. 149-300. Cold Spring Harbor Laboratory Press.
Gatt, M. K. and Glover, D. M. (2006). The Drosophila phosphatidylinositol transfer protein encoded by vibrator is essential to maintain cleavage-furrow ingression in cytokinesis. *J. Cell Sci.* **119**, 2225-2235.
Gatti, M., Giansanti, M. G. and Bonaccorsi, S. (2000). Relationships between the central spindle and the contractile ring during cytokinesis in animal cells. *Microsc. Res. Tech.* **49**, 202-208.
Giansanti, M. G. and Fuller, M. T. (2012). What Drosophila spermatocytes tell us about the mechanisms underlying cytokinesis. *Cytoskeleton* **69**, 869-881.
Giansanti, M. G., Bonaccorsi, S., Williams, B., Williams, E. V., Santolamazza, C., Goldberg, M. L. and Gatti, M. (1998). Cooperative interactions between the central spindle and the contractile ring during Drosophila cytokinesis. *Genes Dev.* **12**, 396-410.
Giansanti, M. G., Farkas, R. M., Bonaccorsi, S., Lindsley, D. L., Wakimoto, B. T., Fuller, M. T. and Gatti, M. (2004). Genetic dissection of meiotic cytokinesis in Drosophila males. *Mol. Biol. Cell* **15**, 2509-2522.
Giansanti, M. G., Bonaccorsi, S., Kurek, R., Farkas, R. M., Dimitri, P., Fuller, M. T. and Gatti, M. (2006). The class I PITP giotto is required for Drosophila cytokinesis. *Curr. Biol.* **16**, 195-201.
Giansanti, M. G., Belloni, G. and Gatti, M. (2007). Rab11 is required for membrane trafficking and actomyosin ring constriction in meiotic cytokinesis of Drosophila males. *Mol. Biol. Cell* **18**, 5034-5047.
Gregory, S. L., Shandala, T., O'Keefe, L., Jones, L., Murray, M. J. and Saint, R. (2007). A Drosophila overexpression screen for modifiers of Rho signalling in cytokinesis. *Fly* **1**, 13-22.
Halachmi, N., Feldman, M., Kimchie, Z. and Lev, Z. (1995). Rop and Ras2, members of the Sec1 and Ras families, are localized in the outer membranes of labyrinthine channels and vesicles of Drosophila nephrocyte, the Garland cell. *Eur. J. Cell Biol.* **67**, 275-283.
Halfon, M. S., Gisselbrecht, S., Lu, J., Estrada, B., Keshishian, H. and Michelson, A. M. (2002). New fluorescent protein reporters for use with the Drosophila Gal4 expression system and for vital detection of balancer chromosomes. *Genesis* **34**, 135-138.
Harrison, S. D., Broadie, K., van de Goor, J. and Rubin, G. M. (1994). Mutations in the Drosophila Rop gene suggest a function in general secretion and synaptic transmission. *Neuron* **13**, 555-566.
Hickson, G. R. X. and O'Farrell, P. H. (2008). Rho-dependent control of anillin behavior during cytokinesis. *J. Cell Biol.* **180**, 285-294.
Hyodo, T., Ito, S., Hasegawa, H., Asano, E., Maeda, M., Urano, T., Takahashi, M., Hamaguchi, M. and Senga, T. (2012). Misshapen-like kinase 1 (MINK1) is a novel component of striatin-interacting phosphatase and kinase (STRIPAK) and is required for the completion of cytokinesis. *J. Biol. Chem.* **287**, 25019-25029.
Jantsch-Plunger, V. and Glotzer, M. (1999). Depletion of syntaxins in the early Caenorhabditis elegans embryo reveals a role for membrane fusion events in cytokinesis. *Curr. Biol.* **9**, 738-745.
Jürgens, G. (2005). Plant cytokinesis: fission by fusion. *Trends Cell Biol.* **15**, 277-283.
Karess, R. E., Chang, X.-j., Edwards, K. A., Kulkarni, S., Aguilera, I. and Kiehart, D. P. (1991). The regulatory light chain of nonmuscle myosin is encoded by spaghetti-squash, a gene required for cytokinesis in Drosophila. *Cell* **65**, 1177-1189.
Langley, A. R., Smith, J. C., Stemple, D. L. and Harvey, S. A. (2014). New insights into the maternal to zygotic transition. *Development* **141**, 3834-3841.
Li, W. M., Webb, S. E., Lee, K. W. and Miller, A. L. (2006). Recruitment and SNARE-mediated fusion of vesicles in furrow membrane remodeling during cytokinesis in zebrafish embryos. *Exp. Cell Res.* **312**, 3260-3275.
Lin, L. and Fisher, P. A. (1990). Immunoaffinity purification and functional characterization of interphase and meiotic Drosophila nuclear lamin isoforms. *J. Biol. Chem.* **265**, 12596-12601.
Low, S. H., Li, X., Miura, M., Kudo, N., Quiñones, B. and Weimbs, T. (2003). Syntaxin 2 and endobrevin are required for the terminal step of cytokinesis in mammalian cells. *Dev. Cell* **4**, 753-759.
Mao, Y. and Baum, B. (2015). Tug of war—the influence of opposing physical forces on epithelial cell morphology. *Dev. Biol.* **401**, 92-102.
Martineau, S. N., Andreassen, P. R. and Margolis, R. L. (1995). Delay of HeLa cell cleavage into interphase using dihydrocytochalasin B: retention of a postmitotic spindle and telophase disc correlates with synchronous cleavage recovery. *J. Cell Biol.* **131**, 191-205.
McKay, H. F. and Burgess, D. R. (2011). 'Life is a highway': membrane trafficking during cytokinesis. *Traffic* **12**, 247-251.
Merrill, P. T., Sweeton, D. and Wieschaus, E. (1988). Requirements for autosomal gene activity during precellular stages of Drosophila melanogaster. *Development* **104**, 495-509.
Park, M., Touihri, S., Müller, I., Mayer, U. and Jürgens, G. (2012). Sec1/Munc18 protein stabilizes fusion-competent syntaxin for membrane fusion in Arabidopsis cytokinesis. *Dev. Cell* **22**, 989-1000.
Piekny, A. J. and Glotzer, M. (2008). Anillin is a scaffold protein that links RhoA, actin, and myosin during cytokinesis. *Curr. Biol.* **18**, 30-36.
Rappaport, R. (1996). *Cytokinesis in Animal Cells*. Cambridge, NY, USA: Cambridge University Press.
Robinett, C. C., Giansanti, M. G., Gatti, M. and Fuller, M. T. (2009). TRAPPII is required for cleavage furrow ingression and localization of Rab11 in dividing male meiotic cells of Drosophila. *J. Cell Sci.* **122**, 4526-4534.
Rothwell, W. F. and Sullivan, W. (2000). Fluorescent analysis of Drosophila embryos. In *Drosophila Protocols* (ed. W. Sullivan, M. Ashburner and R. S. Hawley), pp. 141-158. Cold Spring Harbor: Cold Spring Harbor Laboratory Press.
Royou, A., Field, C., Sisson, J. C., Sullivan, W. and Karess, R. (2004). Reassessing the role and dynamics of nonmuscle myosin II during furrow formation in early Drosophila embryos. *Mol. Biol. Cell* **15**, 838-850.
Salzberg, A., Cohen, N., Halachmi, N., Kimchie, Z. and Lev, Z. (1993). The Drosophila Ras2 and Rop gene pair: a dual homology with a yeast Ras-like gene and a suppressor of its loss-of-function phenotype. *Development* **117**, 1309-1319.
Schiel, J. A., Simon, G. C., Zaharris, C., Weisz, J., Castle, D., Wu, C. C. and Prekeris, R. (2012). FIP3-endosome-dependent formation of the secondary ingression mediates ESCRT-III recruitment during cytokinesis. *Nat. Cell Biol.* **14**, 1068-1078.
Schulze, K. L., Littleton, J. T., Salzberg, A., Halachmi, N., Stern, M., Lev, Z. and Bellen, H. J. (1994). Rop, a Drosophila homolog of yeast Sec1 and vertebrate n-Sect/Munc-18 proteins, is a negative regulator of neurotransmitter release in vivo. *Neuron* **13**, 1099-1108.
Sedzinski, J., Biro, M., Oswald, A., Tinevez, J.-Y., Salbreux, G. and Paluch, E. (2011). Polar actomyosin contractility destabilizes the position of the cytokinetic furrow. *Nature* **476**, 462-466.
Simpson, L. and Wieschaus, E. (1990). Zygotic activity of the nullo locus is required to stabilize the actin-myosin network during cellularization in Drosophila. *Development* **110**, 851-863.
Skop, A. R., Bergmann, D., Mohler, W. A. and White, J. G. (2001). Completion of cytokinesis in C. elegans requires a brefeldin A-sensitive membrane accumulation at the cleavage furrow apex. *Curr. Biol.* **11**, 735-746.
Skop, A. R., Liu, H., Yates, J., III, Meyer, B. J. and Heald, R. (2004). Dissection of the mammalian midbody proteome reveals conserved cytokinesis mechanisms. *Science* **305**, 61-66.
Slack, C., Somers, W. G., Sousa-Nunes, R., Chia, W. and Overton, P. M. (2006). A mosaic genetic screen for novel mutations affecting Drosophila neuroblast divisions. *BMC Genet.* **7**, 33.
Smith, T. C., Fang, Z. and Luna, E. J. (2010). Novel interactors and a role for supervillin in early cytokinesis. *Cytoskeleton* **67**, 346-364.
Somma, M. P., Fasulo, B., Cenci, G., Cundari, E. and Gatti, M. (2002). Molecular dissection of cytokinesis by RNA interference in Drosophila cultured cells. *Mol. Biol. Cell* **13**, 2448-2460.
Straight, A. F., Cheung, A., Limouze, J., Chen, I., Westwood, N. J., Sellers, J. R. and Mitchison, T. J. (2003). Dissecting temporal and spatial control of cytokinesis with a myosin II Inhibitor. *Science* **299**, 1743-1747.
Straight, A. F., Field, C. M. and Mitchison, T. J. (2005). Anillin binds nonmuscle myosin II and regulates the contractile ring. *Mol. Biol. Cell* **16**, 193-201.
Sudhof, T. C. and Rothman, J. E. (2009). Membrane fusion: grappling with SNARE and SM proteins. *Science* **323**, 474-477.
Tomancak, P., Beaton, A., Weiszmann, R., Kwan, E., Shu, S., Lewis, S. E., Richards, S., Ashburner, M., Hartenstein, V., Celniker, S. E. et al. (2002). Systematic determination of patterns of gene expression during Drosophila embryogenesis. *Genome Biol.* **3**, research0088.1.
Toonen, R. F., Kochubey, O., de Wit, H., Gulyas-Kovacs, A., Konijnenburg, B., Sørensen, J. B., Klingauf, J. and Verhage, M. (2006). Dissecting docking and tethering of secretory vesicles at the target membrane. *EMBO J.* **25**, 3725-3737.
Tram, U., Riggs, B., Koyama, C., Debec, A. and Sullivan, W. (2001). Methods for the study of centrosomes in Drosophila during embryogenesis. *Methods Cell Biol.* **67**, 113-123.
VerPlank, L. and Li, R. (2005). Cell cycle-regulated trafficking of Chs2 controls actomyosin ring stability during cytokinesis. *Mol. Biol. Cell* **16**, 2529-2543.
Waizenegger, I., Lukowitz, W., Assaad, F., Schwarz, H., Jürgens, G. and Mayer, U. (2000). The Arabidopsis KNOLLE and KEULE genes interact to promote vesicle fusion during cytokinesis. *Curr. Biol.* **10**, 1371-1374.

Journal of Cell Science

Wieschaus, E. and Sweeton, D. (1988). Requirements for X-linked zygotic gene activity during cellularization of early Drosophila embryos. *Development* **104**, 483-493.

Wilson, G. M., Fielding, A. B., Simon, G. C., Yu, X., Andrews, P. D., Hames, R. S., Frey, A. M., Peden, A. A., Gould, G. W. and Prekeris, R. (2005). The FIP3-Rab11 protein complex regulates recycling endosome targeting to the cleavage furrow during late cytokinesis. *Mol. Biol. Cell* **16**, 849-860.

Wu, M. N., Littleton, J. T., Bhat, M. A., Prokop, A. and Bellen, H. J. (1998). ROP, the Drosophila Sec1 homolog, interacts with syntaxin and regulates neurotransmitter release in a dosage-dependent manner. *EMBO J.* **17**, 127-139.

Zhang, Y. Q., Rodesch, C. K. and Broadie, K. (2002). Living synaptic vesicle marker: synaptotagmin-GFP. *Genesis* **34**, 142-145.

Zhang, X., Bedigian, A. V., Wang, W. and Eggert, U. S. (2012). G protein-coupled receptors participate in cytokinesis. *Cytoskeleton* **69**, 810-818.